Efficient Self-Assembly Synthesis of Uniform CdS Spherical Nanoparticles-Au Nanoparticles Hybrids with Enhanced Photoactivity

*Sancan Han, Linfeng Hu, Nan Gao, Ahmed A. Al-Ghamdi, and Xiaosheng Fang**

The treatment of environmental pollution has become one of the most critical issues in the world. Despite the progress made in the study of semiconductor photocatalysis, it is still a challenge to obtain photocatalysts with high activity through relatively simple fabrication processes. In this work, monodisperse CdS spherical nanoparticles (SNPs) of various sizes and good crystallinity are obtained by only adjusting the starting ratio of reactants and the reaction temperature, exhibiting high photocatalytic performances. The photocatalytic rate constant of the ≈ 100 nm CdS SNPs, especially, is more than double that of P25. Furthermore, 3-mercaptopropyltrimethoxysilane is used to assist the interaction between ≈ 200 nm CdS SNPs and citrate-stabilized Au nanoparticles (NPs). The significant increase of photocatalytic activity is confirmed by the degradation of Rodamine B (RhB) under Xe light irradiation. At the optimal Au concentration (0.5 wt%), the prepared nanohybrids show the highest photocatalytic activity, exceeding that of pure CdS two times. The superior photocatalytic performances of the CdS SNPs-Au nanohybrids can be attributed to the intimate interfacial contact between CdS SNPs and Au NPs, which is a contributing factor to the improvement of transfer and the fate of photogenerated charge carriers from CdS SNPs to Au NPs.

1. Introduction

With the growth of worldwide industry, the severe environmental pollutions have become a major concern of the society. Nanostructured semiconductor photocatalysts have received widespread attention due to their unique physical and chemical properties favored for degradation of organic pollutants and hydrogen production through light.[1–4] Especially, oxide semiconductors such as TiO_2,[5,6] have been particularly regarded as suitable photocatalytic materials during the past two decades because of the high stability, low cost, and strong oxidizing power. However, the high recombination ratios of photoinduced electron–hole pairs and poor response to visible light (the photocatalysis of TiO_2 can only be activated by the UV light which account for about only about 3–5% of total solar irriadiation spectrum) have hindered the application of TiO_2 in photocatalysis.[7] With a bandgap of ≈ 2.4 eV, which corresponds well with the spectrum of sunlight, CdS is one of the reliable semiconductors studied and is probably one of the most important materials in photocatalysis,[8] due to the relative low function, excellent transportion, the direct bandgap, and high electronic mobility.[9,10] Result from the unique morphology-dependent optical and electrical properties, there have been intensive efforts to synthesize CdS nanostrutures with controlled shapes and size,[11] however, up to now investigations about pure CdS suffer from a low photocatalytic efficiency,[12] because of the rapid recombination of the photogenerated electrons and holes. For example, Wang et al.[12a] reported that it took 4 h to complete the degradative process, while Hao et al.[12b] observed only 70% degradation could be achieved after 5 h reaction. Therefore, the synthesis of CdS with high crystallinity and morphological control, which will lead to the high photoactivity, have been pursued for decades. So most of the studies concerning CdS at current stage are focused on the enhancement of photocatalytic efficiencies by preparing hybrids.[13–16]

Indeed, the past few years have witnessed immense interest in nanoscaled hybrids containing both semiconductors and metallic domains,[17–21] aiming to enhance the charge separation and transportation, prolong the functional lifetime, and thus improve the photoactivity toward degradation of pollutants in water. It has been demonstrated that, deposition of noble-metal cocatalyst (Pt or Au) onto semiconductor nanostructure increases the application potentials for photocatalysis.[22] To date, the semiconductor heterostucture (TiO_2-CdS) loaded with nobel metals, alters the efficiency in hydrogen production.[23,24] However, the study on the hybrid nanostructure of CdS-Au with high photoactivity has not been practically carried out, other than the theoretical research on photoinduced charge separation of CdS-Au core-shell nanostructures.[25,26] It remains a significant challenge to integrate highly disparate metal and semiconductor materials together at the nanoscale with well-defined size, morphology and interface, which are critical for the efficient charge cascading process in photocatalytic reactions.

S. C. Han, Prof. L. F. Hu, Dr. N. Gao, Prof. X. S. Fang
Department of Materials Science
Fudan University
Shanghai 200433, P. R. China
E-mail: xshfang@fudan.edu.cn
Dr. A. A. Al-Ghamdi
Physics Department
Faculty of Science
King Abdulaziz University
Jeddah, Saudi Arabia

DOI: 10.1002/adfm.201400012

Therefore, it is necessarily crucial to explore the methodologies to effectively fabricate the hybrid nanostructure of CdS-Au. In fact, no photocatalytic system based on the heterostructure CdS spherical nanoparticles (SNPs) and Au nanoparticles (NPs) with simple self-assembly strategy has been reported to date. It is nummerically demonstrated that the photoluminescence (PL) behaviors of semiconductors can be altered by the surface plasmons of the metallic components,[27] in this work, the enhancement and quenching of the PL intensity in semiconductor-metal heterostructure are explained in terms of the combinative effect of the surface plasmon resonance (SPR) and the Coulomb interaction based on experimental results.

Monodisperse CdS SNPs with different size are obtained through a slightly modified hydrothermal method which is facile and straightforward,[28] and the obtained CdS SNPs show relatively high crystallinity and optimized photocatalytic properties. Motivated by the discovery of the better photoactivity of the semiconductor-metal nanoheterostructure, we have concentrated on the CdS-Au hybrids. 3-mercaptopropyltrimethoxysilane (MPTES) is used to modify the surface of obtained CdS SNPs, triggering successful homogeneous decoration of Au NPs through gold-sulfur bonding interactions. Accordingly, this approach meets the needs for reliable interfacial contact between the semiconductor and the Au NP. As a matter of fact, until now, it is the first time that report on synthesis of uniform CdS SNPs-Au NPs hybrids by such a simple self-assembly strategy is proposed. The photocatalytic efficiency of the hybrid photocatalysts toward Rodamine B (RhB) is also examined, and the significant enhancement of photocatalytic activity observed in the photodegradation indicates double increased photocatalytic rate constant with respect to that of pure CdS SNPs. This work thus provides a simple and low-cost method to synthesize the metal-semiconductor hybrids, which show great potentials for application in photocatalysts, nonlinear optical instruments, photovoltaic devices, and chemical sensors.

2. Result and Discussion

The field-emission scanning electron microscopy (FESEM) images of the CdS SNPs are depicted in **Figure 1**. The CdS SNPs were formed in the solution during the hydrothermal reaction with different starting ratios of the cadmium acetate to thiourea, which were 1:4, 1:10, 1:15, and 1:30, respectively (A–D). Interestingly, the size of the as-formed CdS SNPs was dependent on the starting ratio of cadmium acetate to thiourea; as the starting ratio of cadmium acetate to thiourea increased, the size of the CdS SNPs became smaller. For instance, the sizes of the CdS SNPs prepared at the starting ratio of 1:4, 1:10, 1:15 and 1:30 were ≈ 350 nm, ≈ 200 nm, ≈ 150 nm, ≈ 100 nm, respectively.

In the reaction system, thiourea played important roles during the formation of the CdS SNPs-source of sulfur after

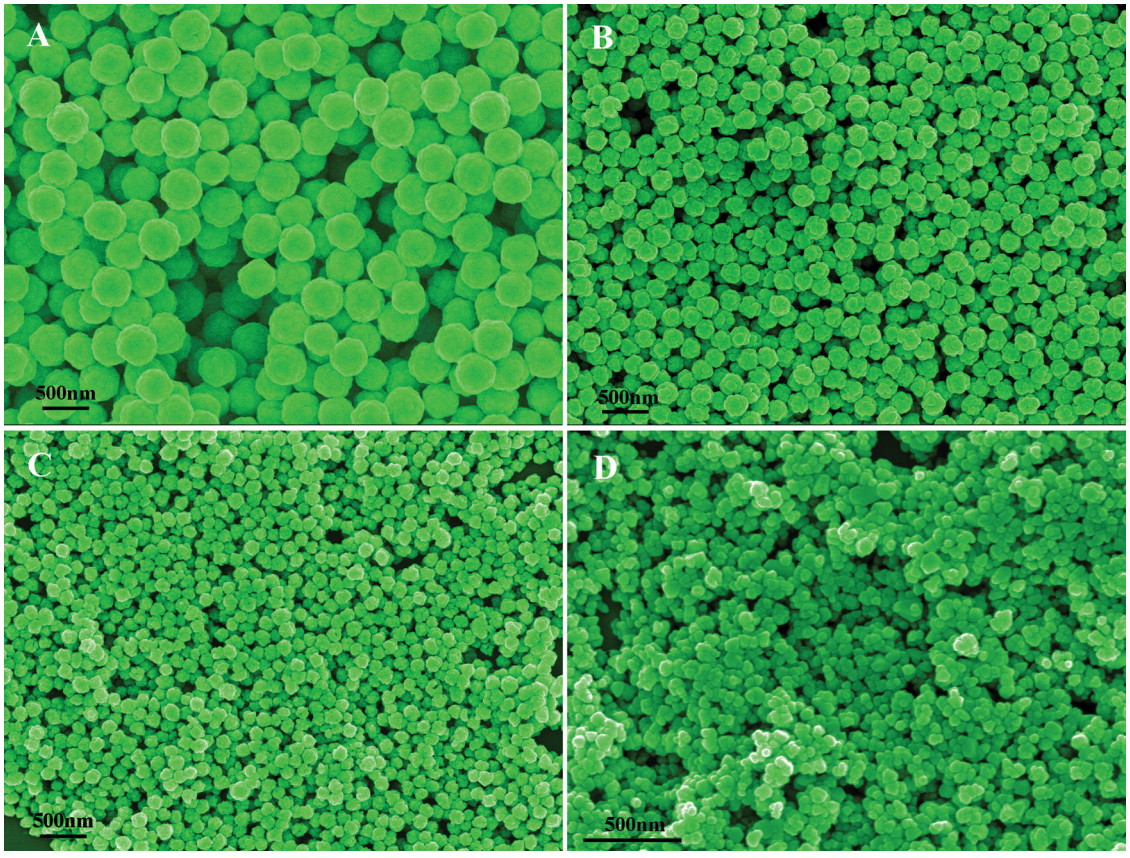

Figure 1. A–D) SEM images of the samples synthesized with different starting ratio of the cadmium acetate to thiourea at 200 °C for 5 h reaction time: A) 1:4, B) 1:10, C) 1:15, D) 1:30.

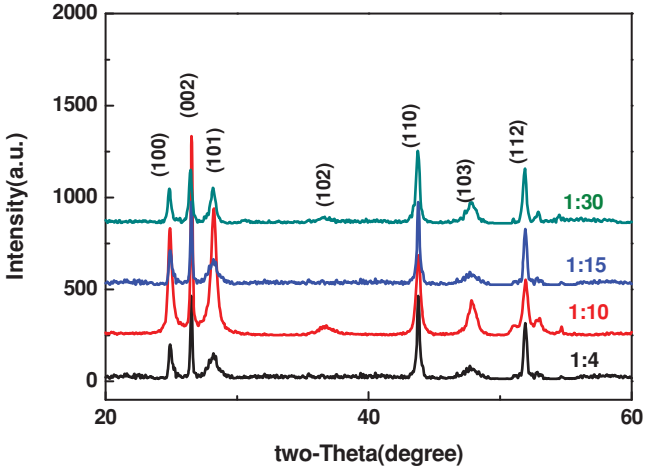

Figure 2. XRD patterns of the CdS SNPs obtained by different starting ratio of the cadmium acetate to thiourea of 1:4, 1:10, 1:15 and 1:30 (as indicated), at 200 °C for 5 h.

the breaking of C = S double bond by the attack of the strong nucleophilic O atoms of H_2O molecules.[28,29] Because of a large excess of thiourea, the Cd atoms on the surface of the formed CdS nanocrystallites could be coordinated with the excess thiourea, resulting in the restricted growth of CdS nanocrystallites, and the same as the size of the CdS SNPs. Then, the aggregation of individual nanocrystallites happened to form CdS SNPs, which was driven by the mechanisms of the partial removal of the stabilizing agents from the nanocrystallite surfaces and surface energy minimization.[28,30]

The X-ray diffraction (XRD) patterns of the CdS SNPs with different size are depicted in **Figure 2**. All the diffraction peaks are assigned to the hexagonal phase of wurtzite CdS structure (JCPDS card No. 75–1545) with the lattice parameters of a = 4.13 Å and c = 6.71 Å, revealing no obvious indication of impurities. To study the influence of the reaction temperature on the formation and structure of CdS SNPs, the morphology of the CdS SNPs formed under the reaction temperatures of 140 °C to 160 °C, 180 °C, and 200 °C are showed in **Figure 3**A–D, respectively. It is noticed that despite of the similar sizes of the obtained CdS SNPs, the shapes of the samples were fairly varied. With the increase of reaction temperature, the surface morphology of the CdS SNPs became rougher. At 140 °C, relatively smooth surfaces of solid spherical samples can be seen from the SEM image. To the contrary, with the reaction temperature increased to 200 °C, the surface of the products was considerably rough, appearing flower-like. The inset of Figure 3D displays the detailed characteristics of the novel architecture. It is yet to be noted that however different the reaction temperatures were, the obtained CdS SNPs were monodisperse, well-defined, regularly structured. As demonstrated through XRD pattern (Figure 3E), by increasing the reaction temperature from 140 °C to 200 °C, the peaks of the crystallinity became stronger, when the reaction temperature raised to 200 °C, the obtained products showed the highest crystallinity. This is possiblly because at higher reaction temperature, thiourea decomposed faster and the nanocrystallites grew at a relatively higher rate to larger sizes, and then the formed CdS SNPs had sufficient time during the hydrothermal process to recrystallize, hence the high reaction temperature benefited the crystallinity improvement of CdS SNPs. And the enhanced crystallinity of semiconductors will be in favor of charge transport and thus increase the photocatalysis activity.[31] We also performed time-resolved investigation on the crystallinity of the CdS SNPs, it was found that the reaction time exceeding 5 hours showed no fundamental effect on the crystallinity.

The photocatalytic activity of CdS SNPs with different starting ratio of cadmium acetate to thiourea has been explored through photodegradation of RhB, as shown in **Figure 4**. All the measurements were conducted under the same conditions, the values of RhB concentration were taken from absorbance at 550 nm, which is its absorption peak and not overlapped with the CdS absorption peaks. In Figure 4A, the rate of degradation C/C_0 of RhB was plotted against the reaction time. With the starting ratio increased, the size of the CdS SNPs decreased, and the rate of RhB degradation increased. The samples of starting ratios of 1:15 and 1:30 with the size of ≈ 150 nm and ≈ 100 nm showed very fast photocatalytic kinetics. Within 10 min, about 80% and 89% of the RhB were decomposed, correspondingly, the rate constants of degradation of RhB were almost two and four times higher than that by Degussa P25 TiO_2 (P25), respectively. The sample of the starting ratio of 1:10 with the size of ≈ 200 nm showed comparable photocatalytic properties with P25 (as summarized in **Table 1**). Only the CdS SNPs with the size of ≈ 350 nm showed a rather lower photocatalytic performance, yet, only 60 min were needed for the catalysts to achieve such degradation. In general, for a given volume, a larger surface area can offer more active adsorption sites and photocatalytic reaction centers, and this means the higher specific surface area will result in the higher photocatalytic activity.[32] As depicted above, the enhancement in the starting ratios of thiourea to cadmium acetate along with an increase in the CdS SNPs size will result in a corresponding increase in specific surface area, and therefore shorten the route for photoinduced electron to migrate to the surface. Taking this into account, the enhancement in photoactivity is attributed to the smaller size of CdS SNPs along with the higher specific surface. Figure 4B shows the UV-visible absorption spectral changes observed of the RhB solution containing the CdS SNPs with the starting ratio of 1:10, which were comparable with that of P25. It is understood the loading of metal cocatalysts allows rapid interfacial electron transfer from the excited semiconductors to the metal, which retards the recombination of photogenerated electron-hole pairs and thereby promotes photocatalytic efficiency. The deposition of the Au NPs onto CdS SNPs with the starting ratios of 1:10 was carried out to promote the photocatalytic performance.

A brief growth mechanism for the present Au-decorated CdS SNPs is proposed and illustrated in **Scheme 1**. In the beginning, positively charged –SH groups are formed on the surface of CdS SNPs. The Au NPs are easily bounded with CdS SNPs through gold–sulfur bonding interactions, and the citrate-stabilized Au NPs with negatively charged surfaces give rise to an increased number of absorbed Au NPs with the positively CdS SNPs because of electrostatically interaction.

Transmission electron microscopy (TEM) images in **Figure 5** show the microscopic morphology and structure of the as-prepared CdS SNPs and CdS SNPs-Au NPs with different weight

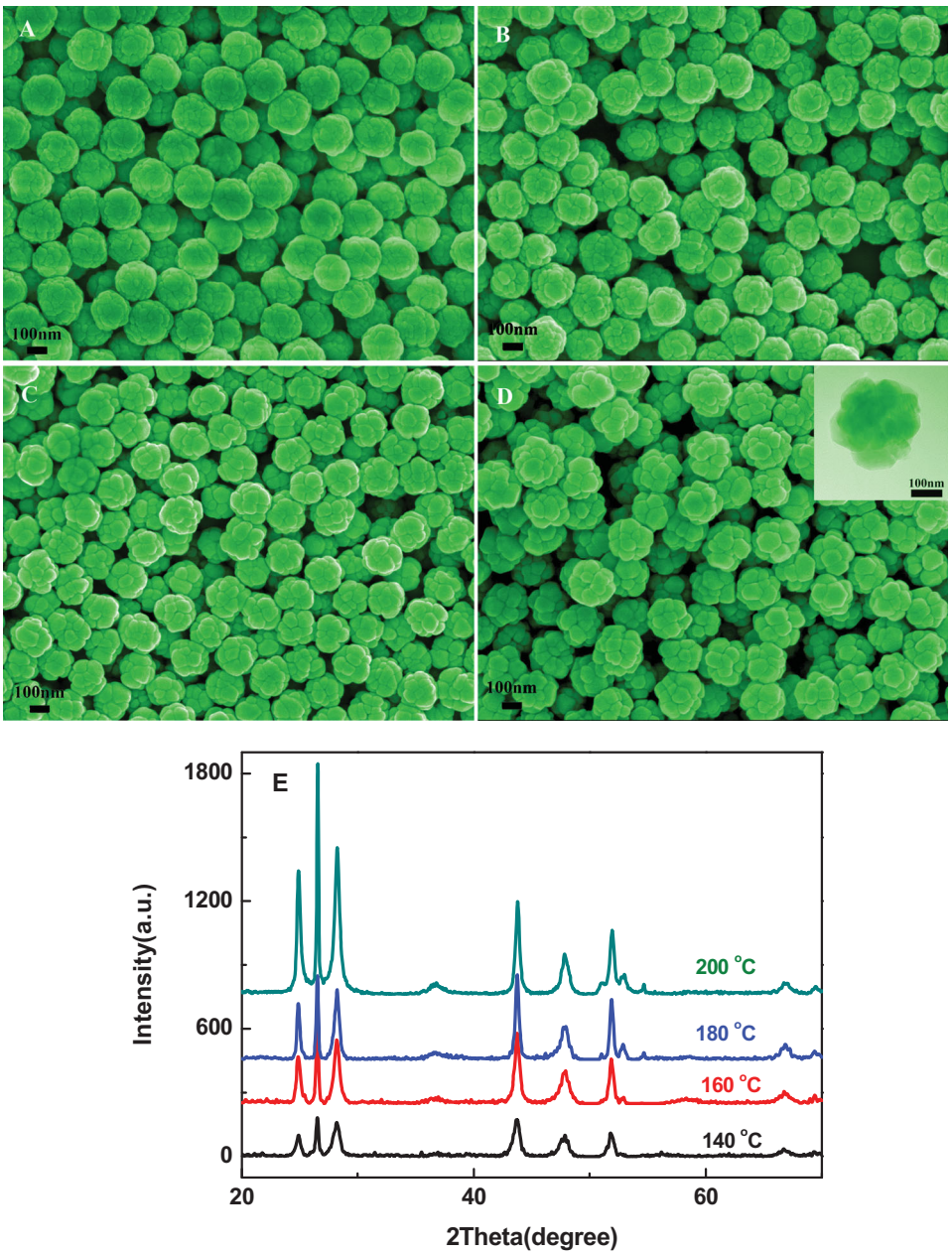

Figure 3. A–D) Low-magnification SEM images reveal well-defined, regularly structured productes at 140 °C, 160 °C, 180 °C, and 200 °C at the starting ratio of cadmium acetate to thiourea of 1:10 for 5 h, respectively. The inset of the D shows corresponding TEM image. (E) The corresponding XRD patterns.

addition ratio of Au NPs. The formation of Au NPs on the surface of CdS SNPs is evident from the TEM images. And with the increase of nominal Au content (wt%) against CdS SNPs in the nanohybrid, the number of Au NPs decorated on the surfaces of the CdS SNPs increased. Figure 5E shows a high-resolution TEM (HRTEM) of a single Au NP. The size of Au NPs was about 25 nm, and the lattice fringes were separated at a distance of 2.32 Å, corresponding to the (111) plane of the fcc cubic of Au NPs. The nanohybrid was further characterized using XRD. As shown in Figure 5E, the peaks of CdS SNPs were observed at 24.9°, 26.5°, 28.2°, 36.6°, 43.7°, 47.8°, and 51.8°, which are indexed to be (100), (002), (101), (102), (110), (103), and (112) planes of CdS SNPs. In addition, characteristic peak at 38.0° that is assigned to the (111) planes of Au NPs with fcc structure can also be observed. However, the intensity of Au NPs in the nanohybrid with a loading of 0.5 wt%, 1.0 wt% was significantly lower, the peak grew rather strong when the loading of Au NPs was increased gradually to 3.0 wt%, which agrees well with TEM observation. To acquire the unique optical characteristic for CdS-Au nanohybrid, their SPR properties were investigated. **Figure 6** shows the UV-visible spectra of the CdS SNPs and the hybrid of CdS SNPs-Au NPs with different weight addition ratios of Au NPs. As for the individually dispersed Au NPs, a strong SPR absorption peak at around 530 nm was shown in

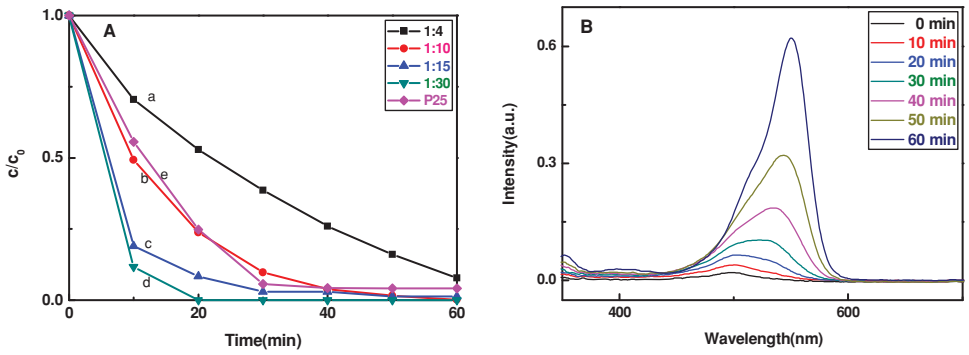

Figure 4. A) Temporal course of the photodegradation of RhB 10 mg L^{-1} in aqueous dispersions of CdS SNPs with different starting ratios of cadmium acetate to thiourea at 200 °C for 5 h and P25 under Xe light irradiation. B) Temporal UV-visible absorption spectral changes observed for RhB solution as a function of irradiation time in the presence of prepared CdS SNPs with the size of ≈ 200 nm.

Table 1. Comparison of the most important photocatalytic parameters during this work.

Sample	Rate constant k [min^{-1}]	Kinetics equation	The rate of degradation in ten minutes $(1 - C/C_0)$
P25	0.0704	$Y = 0.0704x - 0.34765$	0.4438
≈100 nm CdS	0.2330	$Y = 0.2330x - 1.4690$	0.8831
≈150 nm CdS	0.1239	$Y = 0.1239x + 0.13934$	0.8094
≈200 nm CdS	0.0710	$Y = 0.0710x - 0.00310$	0.5072
≈350 nm CdS	0.0318	$Y = 0.0318x + 0.01059$	0.2951
0.5 wt% Au-CdS	0.1423	$Y = 0.1423x + 0.03167$	0.7809
1.0 wt% Au-CdS	0.1054	$Y = 0.1054x + 0.00382$	0.6554
3.0 wt% Au-CdS	0.1090	$Y = 0.1090x - 0.03743$	0.6238

the inset of Figure 6, which consistent with that of Au NPs of ≈ 25 nm.[33] And it can be clearly observed for the series of CdS SNPs-Au NPs nanohybrids that the absorption intensity in the range of 500–700 nm is significantly enhanced by the increase of weight ratios of Au NPs. The increased absorption by field enhancement was calculated based on Maxwell's equation.[34] In fact, as shown in the inset of Figure 6, Au NPs could absorb nearly all the incident light, implying the absorption of CdS SNPs-Au NPs nanohybrids was higher than that of pure CdS SNPs throughout the wavelength range of 200–700 nm. These results reveal that the enhanced absorption ability of the nanohybrid was mainly prompted by the attached Au NPs. Indeed, higher loading of Au NPs led to more absorption of incident light, which benefits the photocatalytic performance.[35,36]

Figure 7 illustrates the PL spectra for pure CdS SNPs and the Au-CdS hybrids containing different weight addition ratios of Au NPs. It is noticed that, the characteristics of the PL spectra of the Au-CdS nanohybrids were very similar to those of pure CdS. Nevertheless, the PL intensity obtained of Au-CdS nanohybrids was weaker than that of CdS SNPs. A similar quenching of PL spectra has been reported,[37] and attributed to the efficient electron transfer from the electronic orbitals below the Fermi level of metal NPs to the semiconductor, which facilitates the separation of photo-induced electron-hole pairs. On the other hand, the enhancement of PL emission of the Au-CdS nanohybrids has also been reported,[33a,38] and explained through the increase of the radiative recombination rate by the surface-plasmon resonance. However, these statements are not sufficiently comprehensive. Generally, there are three crucial fundamental factors for predicting the PL properties of semiconductor-metal NPs hybrids: 1) the increased absorption by field enhancement;[34] 2) the enhancement of radiative recombination rate by surface-plasmon resonance;[39] 3) the increase of nonradiative energy transfer near the metal nanoparticle.[40] These processes collectively determine the PL enhancement and quenching of the semiconductor-metal hybrids. The Coulomb interaction between carriers in different nanoparticles has the usual form shown below: [40]

$$V_{in} = \sum_{i,j} V_{coul}(\vec{R}_i, \vec{R}_j) \quad (1)$$

Where $\vec{R}_i$ is the position of the electron inside the semiconductor nanoparticle participating in the exciton and $\vec{R}_j$ is the position of the carrier inside the metal nanoparticle. The formula shows the intensity of PL

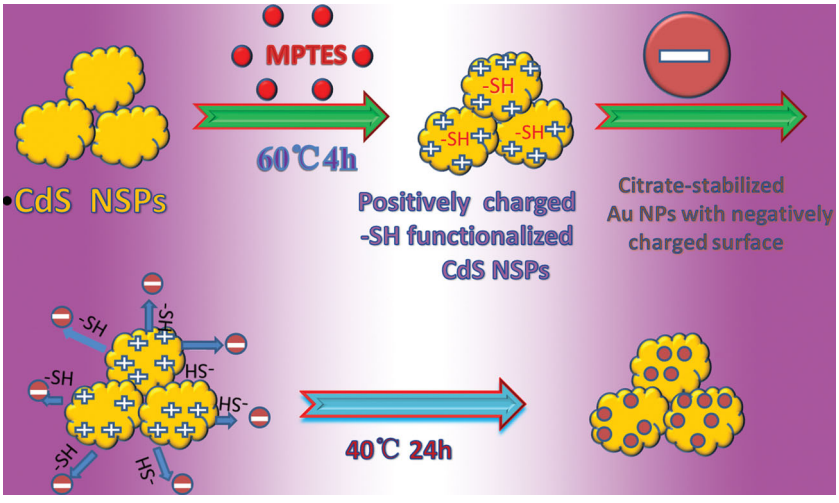

Scheme 1. Schematic illustration for the synthesis of CdS SNPs-Au NPs hybrids by using an Au–SH bonding method.

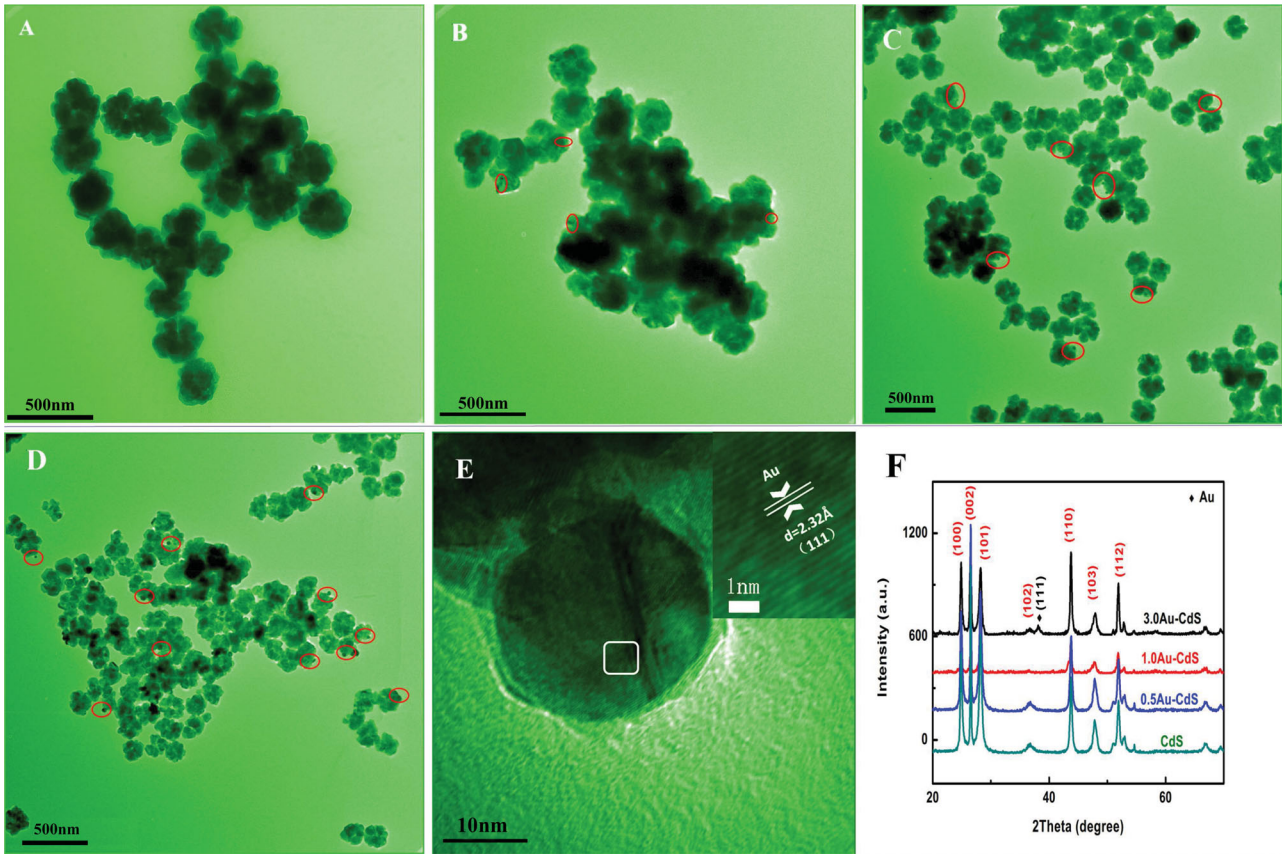

Figure 5. Typical TEM images of the as-prepared samples of A) CdS SNPs and B–D) CdS SNPs-Au NPs hybrids with different weight addition ratios of Au NPs, which correspond to CdS SNPs-Au NPs (0.5 wt%), CdS SNPs-Au NPs (1 wt%), CdS SNPs-Au NPs (3 wt%), respectively. The inside of red circles in (B–D) refers to the Au NPs. E) The high resolution of a single Au nanoparticle, the inset conrresponds to the lattice fringes of the white frame. F) XRD patterns of the prepared CdS SNPs and CdS SNPs-Au NPs hybrids with different weight addition ratios of Au NPs.

is dependent on the distance between the semiconductor and metals NPs. Despite of the Coulomb interaction, which leads to the change in the intensity of PL, surface plasmon in metal NPs is supposed to be more dominant in the intensity of PL. Using the radiating plasmon model, Lakowicz[41] has explained that the surface plasmon resomance (SPR) scattering of metal NPs can enhance the PL emission, while the surface plasmon absorption triggers the quenching effect. The average sizes of

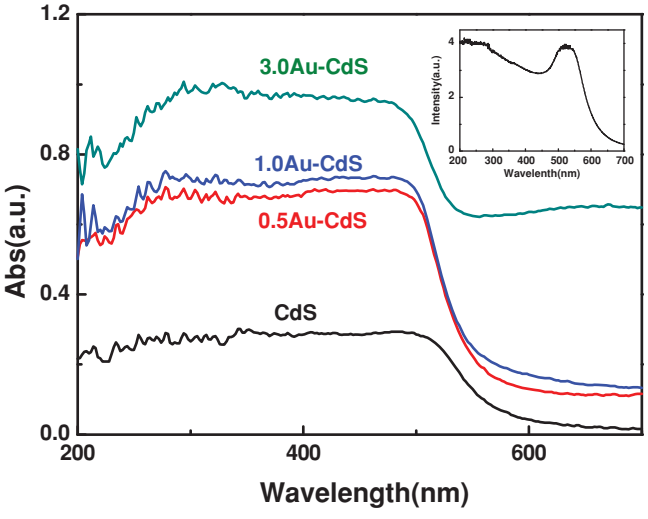

Figure 6. UV-visible absorption spectra of CdS SNPs with different weight addition ratios of Au NPs. The spectrum of pure CdS SNPs was also included for comparison. The inset is the UV-vis absorption spectra of Au NPs.

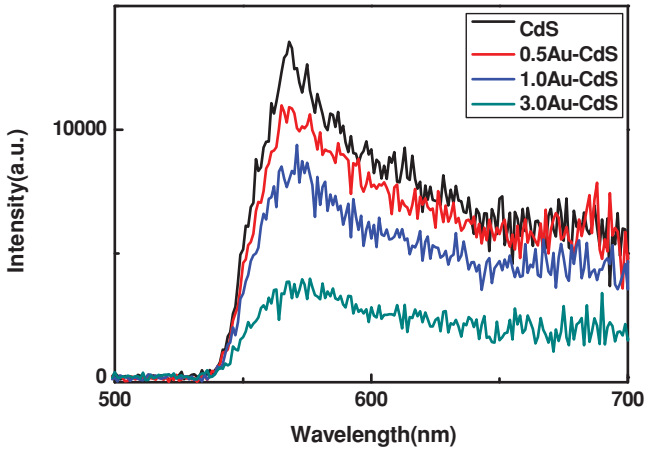

Figure 7. Photoluminescence (PL) spectra of CdS SNPs and CdS SNPs-Au NPs hybrids with different weight addition ratios of Au NPs with an excitation wavelength of 350 nm.

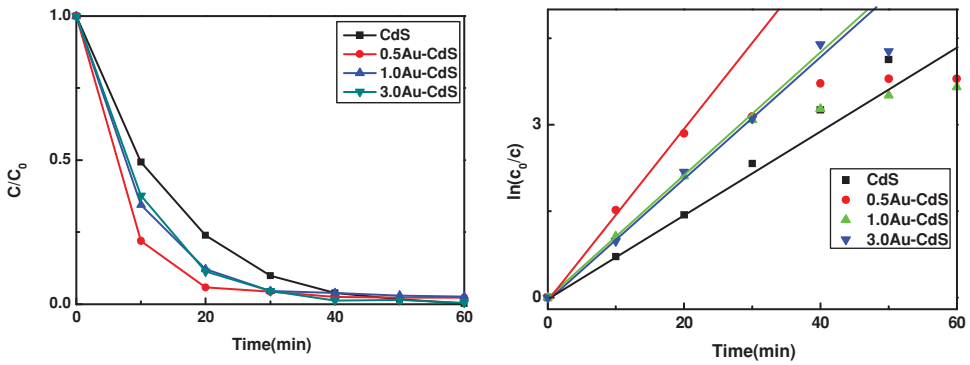

Figure 8. A) Photodegradation and B) the rate of photodegradation of RhB dye in presence of CdS SNPs and CdS SNPs-Au NPs hybrids with different weight addition ratios of Au NPs.

the Au NPs in our hybrid samples were small (≈25 nm), therefore, the absorption dominated over the scattering process. According to the radiating plasmon model of Lakowicz, predicts the quenching of PL, which agrees well with our results shown in Figure 7. To the best of our knowlege, it is the first time that the combination effects on the PL are systematically explained, from the perspect of experimental results. Of course, efficient electron transfer between CdS SNPs and Au NPs is considered as the important factor for the weaking of PL.[37]

As the Au NPs on the surface of CdS SNPs acted as electron traps, our hybrids were expected to work as an efficient photocatalyst. As shown in **Figure 8**, it is clear that all of the CdS SNPs-Au NPs hybrids exhibited higher photocatalytic activities compared with the pure CdS SNPs under Xe light irradiation, which was ascribed to the pronounced charge separation of CdS-Au. In particular, the CdS SNPs with 0.5 wt% Au show the highest catalytic activity, with 78.9% of the RhB decomposed in 10 min. To quantitatively compare the photocatalytic performances of different Au-decorated CdS SNPs samples, the apparent rate constant for RhB photodegradation (k) was computed using the pseudo-first-order approximation, as shown in Figure 8B. As depicted in Table 1, pure CdS showed a relatively low photocatalysis with a rate constant $k = 0.0710\ min^{-1}$. After the introduction of only a small amount of Au, the photoactivity of the CdS SNPs-Au NPs (0.5 wt%) sample was remarkably enhanced and its k value reached $0.1423\ min^{-1}$, exceeding that of pure CdS by a factor of 2, and also doubling that of commercial P25 (As shown in Table 1). Figure 6 shows the higher Au loading of CdS SNPs leads to higher light adsorption, though it is not necessarily true that the more light adsorption, the higher photocatalytic performance. As shown in Figure 8, a further increase in Au content higher than 0.5 wt% leads to the decrease of photocatalytic activity. In general, when the amount of loaded Au is sufficient, the Au NPs can induce effective charge separation, lower down the activation energy, and hence promote the oxidation of organic molecules.[42] However, excesses of Au NPs may deteriorate the catalytic performance by acting as recombination centers.[37b]

On the basis of the above results, it is necessary to discuss the band structure of the CdS SNPs-Au NPs hybrids in detail, which is schematically displayed in **Scheme 2**. The Fermi energy level of Au NPs is lower than that of CdS SNPs,

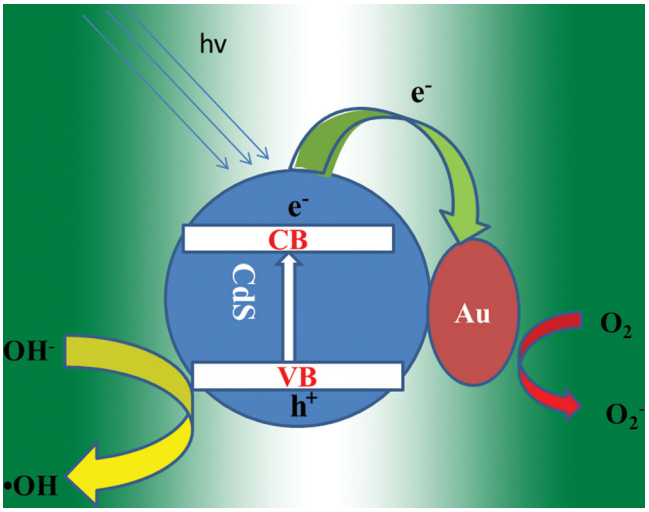

Scheme 2. Schematic illustration of the charge separation at the interface of CdS SNPs-Au NPs hybrids.

and it can lead to the migration of electrons from the conduction band of CdS SNPs to Au NPs in order to achieve the balance in Fermi energy level equilibration. Under Xe light irradiation, electrons in the valence band (VB) of CdS were excited to the conduction band (CB), and meanwhile, the same amount of holes were in the VB. Driven by potential energy, the photogenerated electrons in the CB of CdS SNPs can transfer to Au NPs. Such electron transfer enhances the separation of photoinduced holes and electrons, further prolongs the lifetime of photoinduced pairs,[37] explaining why the intensity of PL decreased. Subsequently, the adsorbed O_2 on the surface of samples can easily trap photoelectrons to produce superoxide anion radicals (O_2^-), and the photoholes left in the VB of CdS SNPs will react with OH^- to generate hydroxy radicals (·OH). As a powerful oxidant, the organic chemicals can be strongly decomposed, and thus increase the photoactivity. In conclusion, it is shown through the photocatalysis results that the appropriate Au content of 0.5 wt% in the CdS-Au hybrids led to the highest photoactivity, resulting effective separation of photoinduced pairs, confirmed by the variation between PL intensity and photocatalytic activities of the samples.

3. Conclusion

A method to produce uniform CdS spherical nanoparticles-Au NP (CdS SNPs-Au NPs) hybrids through a simple self-assembly strategy, in terms of the gold–sulfur bonding interactions, is for the first time proposed. The monodisperse CdS SNPs with different sizes, obtained using the facile hydrothermal synthesis, show excellent photoactivity, which can be further optimized by means of depositing Au NPs. Especially, the photocatalytic performances of CdS SNPs with the sizes of ≈ 150 nm and ≈ 100 nm are considerably better than that of the commercially available P25. Also, the photocatalytic characteristics of pure CdS SNPs and the CdS-Au hybrids with different weight ratios of Au NPs are investigated. The combination effect of the SPR and the coulomb interaction on the quenching and enhancement of PL is also systematically studied. The strategy presented in this work can be extended to the synthesis of other binary semiconductor hybrids.

4. Experimental Section

Typically, 2.4 mmol of $Cd(CH_3COO)_2{\cdot}2H_2O$ (Sinopharm Chemical Reagent Corp.) and 24 mmol of thiourea (Sinopharm Chemical Reagent Corp.) with the starting ratio of cadmium acetate to thiourea of 1:10 were dissolved in 60 mL of deionized water to form a clear solution after stirring for 30 min at room temperature. The solution was then transferred into a 100 mL Teflon-lined stainless steel autoclave. The autoclave was sealed and heated to 200 °C for 5 h and cooled naturally to room temperature after the reaction. The other different sizes of the CdS SNPs were obtained by changing the the starting amount of thiourea as to the ratios of 1:4, 1:15, and 1:30, respectively.

The CdS SNPs-Au NPs nanohybrids were synthesized according to the following procedure. Citrate-stabilized Au NPs were prepared by Dotzauer's method.[43] Firstly, the 100 mL of $HAuCl_4$ aqueous solution (0.04 wt%) was heated to the boil for refluxing under constant stirring. The refluxing was allowed for a few minutes, before 12 mL of 1 wt% sodium citrate aqueous solution was added into aqueous $HAuCl_4$ quickly and kept refluxing for a further 10 min to form homogeneous Au NPs in aqueous solution. The obtained aqueous solution of Au NPs was transfered into a beaker after cooling to room temperature and stored at 8 °C in a refrigerator before use. Then, 0.2 g of CdS SNPs were immersed into 100 mL of ethanol, and MPTES (2 mL) was afterwards added by vigorous stirring at 60 °C for 4 h and then rinsed with DI water and ethanol three times. The freshly washed CdS SNPs were immersed into aqueous solution of Au NPs of the desired volume (Au NPs concentration, 0.16 mg mL^{-1}; citrate concentration, 0.075 mg mL^{-1}) followed by vigorous shaking at 40 °C for 24 h.

Photocatalytic performances were measured by the degradation of RhB under Xe light (350W) irradiation at room temperature after adding 30 mg of the photocatalyst into 60 mL RhB (Rhodamine B) solution (10 mg L^{-1}). The reaction mixture was stirred in the dark for 40 min to achieve the adsorption-desorption equilibrium between RhB and the photocatalyst. Then, the mixture was exposed to the Xe light under constant stirring. After removing the photocatalyst from the mixture solution by centrifugation, the concentrations of the RhB were calculated by measuring the absorbance of RhB at 550 nm.[44]

The morphology, structure, and composition of the samples were analyzed with field-emission scanning electron microscopy (FESEM, JSM-6701F), and transmission electron microscopy (TEM, CM200FEG), and X-ray diffraction using Cu Kα radiation (XRD, Bruker D8-A25). The optical properties of the samples were characterized using a UV-visible spectrophotometer (Hitachi U-4100), and $BaSO_4$ was employed during the measurement as the internal reflectance standard. The fluorescence performance of the samples at room-temperature were characterized using the photoluminescence (PL) spectrofluorometer (Fluoromax-4). The 350 nm emission induced from a He-Cd laser source was used for exciting the samples.

Acknowledgements

The authors thank Profs. Y. F. Mei and Z. Q. Liang from Fudan University for the kind supports on the experimental measurements. This work was supported by the National Natural Science Foundation of China (Grant Nos. 91123006 and 51372040), Shanghai Shu Guang Project (12SG01), Shanghai Pujiang Program (12PJ1400300), Innovation Program of Shanghai Municipal Education Commission (14ZZ003), Science and Technology Commission of Shanghai Municipality (13NM1400300 and 11520706200), the Programs for Professor of Special Appointment (Eastern Scholar) at Shanghai Institutions of Higher Learning and for New Century Excellent Talents in University (NCET-11–0102) and the National Basic Research Program of China (Grant No. 2012CB932303).

Received: January 3, 2014
Revised: January 26, 2014
Published online: March 6, 2014

[1] a) A. Fujishima, *Nature* **1972**, *238*, 37; b) L. W. Zhang, H. B. Fu, Y. F. Zhu, *Adv. Funct. Mater.* **2008**, *18*, 2180; c) J. S. Lee, K. H. You, C. B. Park, *Adv. Mater.* **2012**, *24*, 1084; d) W. B. Hou, S. B. Cronin, *Adv. Funct. Mater.* **2013**, *23*, 1612.

[2] a) J. Z. Zhang, *MRS Bull.* **2011**, *36*, 48; b) D. K. Zhong, D. R. Gamelin, *J. Am. Chem. Soc.* **2010**, *132*, 4202; c) J. Yu, L. Qi, M. Jaroniec, *J. Phys. Chem. C.* **2010**, *114*, 13118; d) M. Barroso, A. J. Cowan, S. R. Pendlebury, M. Grätzel, D. R. Klug, J. R. Durrant, *J. Am. Chem. Soc.* **2011**, *133*, 14868.

[3] a) S. Liu, N. Zhang, Z. R. Tang, Y. J. Xu, *ACS Appl. Mater. Interfaces* **2012**, *4*, 6378; b) T. S. Ahmadi, Z. L. Wang, T. C. Green, A. Henglein, M. A. El-Sayed, *Science* **1996**, 1924; c) X. S. Fang, T. Y. Zhai, U. K. Gautam, L. Li, L. M. Wu, Y. Bando, D. Golberg, *Prog. Mater. Sci.* **2011**, *56*, 175; d) G. P. Xu, S. L. Ji, C. H. Miao, G. D. Liu, C. H. Ye, *J. Mater. Chem.* **2012**, *22*, 4890.

[4] a) X. S. Fang, L. M. Wu, L. F. Hu, *Adv. Mater.* **2011**, *23*, 585; b) Z. Yin, Z. Wang, Y. Du, X. Qi, Y. Huang, C. Xue, H. Zhang, *Adv. Mater.* **2012**, *24*, 5374.

[5] a) J. Du, X. Lai, N. Yang, J. Zhai, D. Kisailus, F. Su, D. Wang, L. Jiang, *ACS Nano* **2010**, *5*, 590; b) Y. Zhang, Z. R. Tang, X. Fu, Y. J. Xu, *ACS Nano* **2011**, *5*, 7426; c) C. Chen, W. Cai, M. Long, B. Zhou, Y. Wu, D. Wu, Y. Feng, *ACS Nano* **2010**, *4*, 6425.

[6] a) B. Y. Xia, B. Wang, H. B. Wu, Z. L. Liu, X. Wang, X. W. Lou, *J. Mater. Chem.* **2012**, *22*, 16499; b) H.-i. Kim, G.-h. Moon, D. Monllor-Satoca, Y. Park, W. Choi, *J. Phys. Chem. C.* **2011**, *116*, 1535; c) H. Zhang, X. Lv, Y. Li, Y. Wang, J. Li, *ACS Nano* **2009**, *4*, 380.

[7] a) H. Kominami, S. Y. Murakami, J. I. Kato, Y. Kera, B. Ohtani, *J. Phys. Chem. B.* **2002**, *106*, 10501; b) J. C. Yu, L. Zhang, Z. Zheng, J. Zhao, *Chem. Mater.* **2003**, *15*, 2280.

[8] a) Y. Guo, J. Wang, Z. Tao, F. Dong, K. Wang, X. Ma, P. Yang, P. Hu, Y. Xu, L. Yang, *CrystEngComm* **2012**, *14*, 1185; b) S. K. Apte, S. N. Garaje, G. P. Mane, A. Vinu, S. D. Naik, D. P. Amalnerkar, B. B. Kale, *Small* **2011**, *7*, 957; c) Y. Guo, L. Wang, L. Yang, J. Zhang, L. Jiang, X. Ma, *Mater. Lett.* **2011**, *65*, 486; d) P. Gao, J. Liu, S. Lee, T. Zhang, D. D. Sun, *J. Mater. Chem.* **2012**, *22*, 2292.

[9] a) T. Y. Zhai, X. S. Fang, L. Li, Y. Bando, D. Golberg, *Nanoscale* **2010**, *2*, 186; b) L. Li, P. C. Wu, X. S. Fang, T. Y. Zhai, L. Dai, M. Y. Liao, Y. Koide, H. Q. Wang, Y. Bando, D. Golberg, *Adv. Mater.* **2010**, *22*, 3161.

[10] Y. F. Lin, J. Song, Y. Ding, S. Y. Lu, Z. L. Wang, *Adv. Mater.* **2008**, *20*, 3127.

[11] a) F. Li, W. Bi, T. Kong, C. Wang, Z. Li, X. Huang, *J. Alloy Compd.* **2009**, *479*, 707; b) B. Pan, Y. Xie, S. Zhang, L. Lv, W. Zhang, *ACS Appl. Mater. Interfaces* **2012**, *4*, 3938.

[12] a) S. Wang, P. Liu, X. Wang, X. Fu, *Langmuir* **2005**, *21*, 11969; b) Q. Hao, J. Xu, X. Zhuang, Q. Zhang, Q. Wan, H. Pan, X. Zhu, A. Pan, *Mater. Lett.* **2013**, *100*, 141.

[13] a) E. Khon, N. N. Hewa-Kasakarage, I. Nemitz, K. Acharya, M. Zamkov, *Chem. Mater.* **2010**, *22*, 5929; b) M. Li, X. F. Yu, S. Liang, X. N. Peng, Z. J. Yang, Y. L. Wang, Q. Q. Wang, *Adv. Funct. Mater.* **2011**, *21*, 1788; c) E. Khon, A. Mereshchenko, A. N. Tarnovsky, K. Acharya, A. Klinkova, N. N. Hewa-Kasakarage, I. Nemitz, M. Zamkov, *Nano. Lett.* **2011**, *11*, 1792.

[14] a) S. Yan, D. Hu, F. Hu, J. Wu, N. Huang, Z. Xiao, *CrystEngComm* **2011**, *13*, 4580; b) F. Zhang, S. Niu, W. Guo, G. Zhu, Y. Liu, X. Zhang, Z. L. Wang, *ACS Nano* **2013**, *7*, 4537; c) Y. Tak, S. J. Hong, J. S. Lee, K. Yong, *J. Mater. Chem.* **2009**, *19*, 5945.

[15] a) A. Ye, W. Fan, Q. Zhang, W. Deng, Y. Wang, *Catal. Sci. Technol.* **2012**, *2*, 969; b) S. Liu, Z. Chen, N. Zhang, Z. R. Tang, Y. J. Xu, *J. Phys. Chem. C.* **2013**, *117*, 8251.

[16] a) K. Wu, H. Zhu, Z. Liu, W. Rodríguez-Córdoba, T. Lian, *J. Am. Chem.Soc.* **2012**, *134*, 10337; b) M. J. Berr, A. Vaneski, C. Mauser, S. Fischbach, A. S. Susha, A. L. Rogach, F. Jäckel, J. Feldmann, *Small* **2012**, *8*, 291; c) K. P. Acharya, R. S. Khnayzer, T. O'Connor, G. Diederich, M. Kirsanova, A. Klinkova, D. Roth, E. Kinder, M. Imboden, M. Zamkov, *Nano. Lett.* **2011**, *11*, 2919.

[17] a) Y. Q. Li, L. Y. Guan, H. L. Zhang, J. Chen, S. Lin, Z. Y. Ma, Y. D. Zhao, *Anal. Chem.* **2011**, *83*, 4103; b) X. Chen, S. Shen, L. Guo, S. S. Mao, *Chem. Rev.* **2010**, *110*, 6503.

[18] T. Mokari, E. Rothenberg, I. Popov, R. Costi, U. Banin, *Science* **2004**, *304*, 1787.

[19] a) W. Shi, H. Zeng, Y. Sahoo, T. Y. Ohulchanskyy, Y. Ding, Z. L. Wang, M. Swihart, P. N. Prasad, *Nano. Lett.* **2006**, *6*, 875; b) K. K. Haldar, G. Sinha, J. Lahtinen, A. Patra, *ACS Appl.Mater. Interfaces* **2012**, *4*, 6266.

[20] a) X. Li, J. Lian, M. Lin, Y. Chan, *J. Am. Chem. Soc.* **2010**, *133*, 672; b) A. Kostopoulou, F. Thétiot, I. Tsiaoussis, M. Androulidaki, P. D. Cozzoli, A. Lappas, *Chem. Mater.* **2012**, *24*, 2722.

[21] a) I. Jen-La Plante, S. E. Habas, B. D. Yuhas, D. J. Gargas, T. Mokari, *Chem. Mater.* **2009**, *21*, 3662; b) L. Zhang, D. A. Blom, H. Wang, *Chem. Mater.* **2011**, *23*, 4587.

[22] a) M. Ye, J. Gong, Y. Lai, C. Lin, Z. Lin, *J. Am. Chem. Soc.* **2012**, *134*, 15720; b) H. Park, Y. K. Kim, W. Choi, *J. Phys. Chem. C* **2011**, *115*, 6141.

[23] a) H. Park, W. Choi, M. R. Hoffmann, *J. Mater. Chem.* **2008**, *18*, 2379; b) J. S. Jang, S. H. Choi, H. G. Kim, J. S. Lee, *J. Phys. Chem. C* **2008**, *112*, 17200.

[24] J. Fang, L. Xu, Z. Zhang, Y. Yuan, S. Cao, Z. Wang, L. Yin, Y. Liao, C. Xue, *ACS Appl. Mater. Interfaces* **2013**, *5*, 8088.

[25] G. P. Li, R. Chen, D. L. Guo, L. M. Wong, S. J. Wang, H. D. Sun, T. Wu, *Nanoscale* **2011**, *3*, 3170.

[26] D. Mongin, E. Shaviv, P. Maioli, A. l. Crut, U. Banin, N. Del Fatti, F. Vallée, *ACS Nano* **2012**, *6*, 7034.

[27] a) A. Akimov, A. Mukherjee, C. Yu, D. Chang, A. Zibrov, P. Hemmer, H. Park, M. Lukin, *Nature* **2007**, *450*, 402; b) Z. K. Zhou, M. Li, Z. J. Yang, X. N. Peng, X. R. Su, Z. S. Zhang, J. B. Li, N. C. Kim, X. F. Yu, L. Zhou, *ACS Nano* **2010**, *4*, 5003.

[28] G. Lin, J. Zheng, R. Xu, *J. Phys. Chem. C* **2008**, *112*, 7363.

[29] Q. Q. Wang, G. Xu, G. R. Han, *Cryst. Growth Des.* **2006**, *6*, 1776.

[30] Z. Zhang, H. Sun, X. Shao, D. Li, H. Yu, M. Han, *Adv. Mater.* **2005**, *17*, 42.

[31] a) S. Ding, X. Yin, X. Lü, Y. Wang, F. Huang, D. Wan, *ACS Appl. Mater. Interfaces* **2011**, *4*, 306; b) S. Biswas, M. Hossain, T. Takahashi, Y. Kubota, A. Fujishima, *Thin Solid Films* **2008**, *516*, 7313; c) X. Lü, S. Ding, Y. Xie, F. Huang, *Eur. J. Inorg. Chem.* **2011**, 2879.

[32] a) W. Wang, J. Yu, Q. Xiang, B. Cheng, *Appl. Catal. B: Environ.* **2012**, *119*, 109; b) D. Chen, F. Huang, Y. B. Cheng, R. A. Caruso, *Adv. Mater.* **2009**, *21*, 2206.

[33] a) P. Guo, J. Xu, X. Zhuang, W. Hu, X. Zhu, H. Zhou, L. Tang, A. Pan, *J. Mater. Chem. C* **2013**, *1*, 566; b) A. C. Templeton, J. J. Pietron, R. W. Murray, P. Mulvaney, *J. Phys. Chem. B* **2000**, *104*, 564.

[34] K. Tanabe, *J. Phys. Chem. C* **2008**, *112*, 15721.

[35] Y. Wu, H. Liu, J. Zhang, F. Chen, *J. Phys. Chem. C* **2009**, *113*, 14689.

[36] C. Wang, L. Yin, L. Zhang, N. Liu, N. Lun, Y. Qi, *ACS Appl. Mater. Interfaces* **2010**, *2*, 3373.

[37] a) X. Xing, R. Liu, X. Yu, G. Zhang, H. Cao, J. Yao, B. Ren, Z. Jiang, H. Zhao, *J. Mater. Chem. A* **2013**, *1*, 1488; b) S. Liu, Y. J. Xu, *Nanoscale* **2013**, *5*, 9330.

[38] D. R. Jung, J. Kim, S. Nam, C. Nahm, H. Choi, J. I. Kim, J. Lee, C. Kim, B. Park, *Appl. Phys. Lett.* **2011**, *99*, 041906.

[39] H. Mertens, A. Koenderink, A. Polman, *Phys. Rev. B* **2007**, *76*, 115123.

[40] A. O. Govorov, G. W. Bryant, W. Zhang, T. Skeini, J. Lee, N. A. Kotov, J. M. Slocik, R. R. Naik, *Nano. Lett.* **2006**, *6*, 984.

[41] J. R. Lakowicz, *Anal. Biochem.* **2005**, *337*, 171.

[42] J. Yang, D. Wang, H. Han, C. Li, *Acc. Chem. Res* **2013**, *46*, 1900.

[43] D. M. Dotzauer, J. Dai, L. Sun, M. L. Bruening, *Nano. Lett.* **2006**, *6*, 2268.

[44] H. S. Wu, L. D. Sun, H. P. Zhou, C. H. Yan, *Nanoscale* **2012**, *4*, 3242.